ADVANCED MATERIALS TECHNOLOGIES
www.advmattechnol.de

# Artificially Weaved Textile-like Surface Micromachined Graphene-Polymer Flexible Bioelectrodes

*Seba Nur Alhasan, S. Sajjad Mirbakht, Saygun Guler, Osman Sahin, Muhammad Umar, Burcu Arman Kuzubasoglu, and Murat Kaya Yapici**

**Dry, flexible, and self-adhesive sensors are critical enablers for wearable, long-term biosignal recording devices. Here, an ultra-thin, flexible textile-like microstructured electrode with self-adhesive abilities is presented for conformal attachment and long-term electrocardiography (ECG) recording. The reported electrode is manufactured using a spin-coatable and electron-beam sensitive formulation of poly (methyl methacrylate) (PMMA) resist, also commonly known as acrylic, which is at the same time a widely-employed material in the textile industry. The textile-like structure of the bioelectrodes with a linewidth of 100 µm and gap size of 100 µm is achieved by patterning PMMA through oxygen plasma and a hard mask layer without requiring complex and expensive e-beam lithography (EBL) processes. Graphene oxide (GO) is introduced to the electrodes as active material followed by a reduction step using eco-friendly pure vitamin C (L-ascorbic acid). The functionality of the reported electrodes is benchmarked against pre-gelled wet Ag/AgCl electrodes, comparing their signal quality and skin-electrode impedance, and achieving a correlation score of 98.84%. Furthermore, it is demonstrated that the electrodes are flexible, water resistant, and can be used multiple times; rendering them suitable for wearable electronics purposes even during intense physical activities both in dry and wet environments.**

## 1. Introduction

Cardiovascular monitoring using electrocardiography (ECG) is a commonly used diagnostic technique with a vast application area in health informatics including identification of acute stress levels,[1] emotion recognition,[2] diagnosis of various cardiac diseases including coronary syndromes and myocardial infarction,[3,4] as well as, determining drug efficiency in treatment.[5] While short-term patient monitoring provides information for some of the aforementioned health issues, many require continuous and long-term tracking of biopotentials for an accurate diagnosis. A typical procedure for acquiring ECG data involves using Ag/AgCl electrodes with adhesive backing for reliable attachment to the skin. Although these wet electrodes have proved highly accurate, they have two fundamental issues: 1) conductive gels degrade over time affecting the signal quality, and 2) strong adhesives induce skin irritation and trauma.[6] Such limitations have led to the rapid growth of dry electrode alternatives which do not require skin preparation and viscous gels prior to use.[7] Eliminating the gel not only resolves skin irritation but also assures reusability over extended durations.

Recently, various types of dry electrodes have been proposed including microneedle type,[8] capacitive,[9] and surface electrodes.[10] Despite their potential side effects, including inflammation,[11] various fabrication strategies were developed to realize microneedle electrodes in an effort to minimize or mitigate motion artifacts by penetrating the outer skin layer.[12] For instance, deep X-ray lithography and copper (Cu) electroplating were used to pattern grooves out of Poly (methyl methacrylate) (PMMA) for brain-computer interface applications.[13] SU-8 microneedle arrays were built for electroencephalogram (EEG) on a flexible polydimethylsiloxane (PDMS) mold with a porous parylene release layer preventing the metal from peeling off of the substrate.[14] Another study proposed a fabrication process where the laser-direct writing (LDW) was used to create pattern on a polyethylene terephthalate (PET) substrate, and the magnetorheological drawing lithography (MRDL) was used for constructing microneedles on top of it.[15] UV maskless lithography was also

S. N. Alhasan, S. S. Mirbakht, S. Guler, O. Sahin, M. Umar, B. Arman Kuzubasoglu, M. K. Yapici
Faculty of Engineering and Natural Sciences
Sabanci University
Istanbul 34956, Türkiye
E-mail: mkyapici@sabanciuniv.edu

M. Umar, B. Arman Kuzubasoglu, M. K. Yapici
Sabanci University SUNUM Nanotechnology Research Center
Istanbul 34956, Türkiye

M. K. Yapici
Department of Electrical and Computer Engineering
University of Washington
Seattle, WA 98195, USA

The ORCID identification number(s) for the author(s) of this article can be found under https://doi.org/10.1002/admt.202402032



**DOI: 10.1002/admt.202402032**

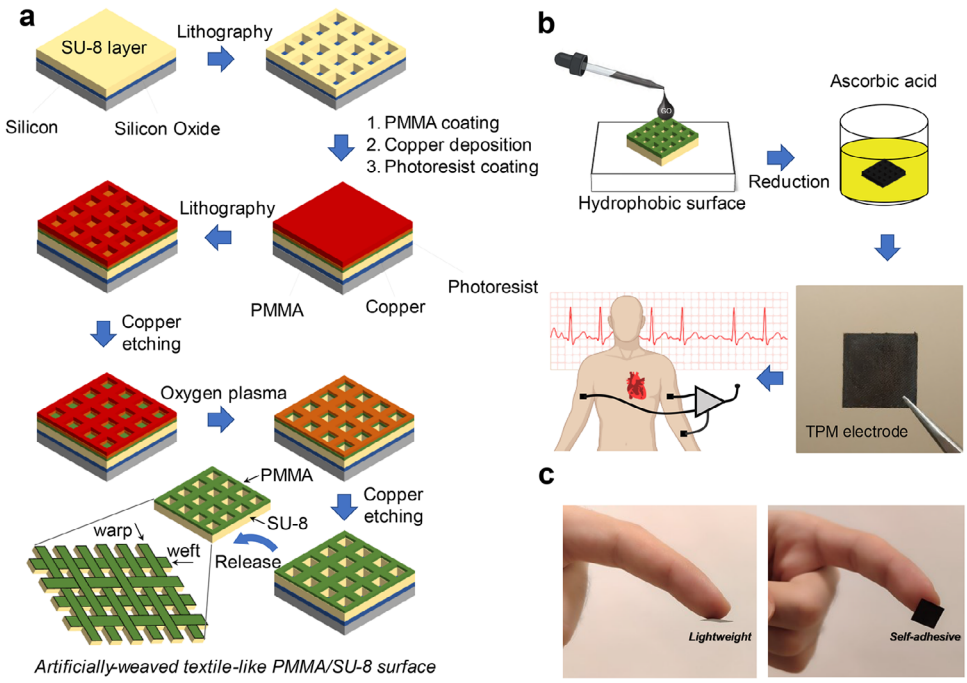


**Figure 1.** a) Fabrication steps of textile-like polymeric (TPM) electrode, b) GO coating-reduction process, and c) Photos of the 1 × 1 cm TPM electrode showcasing its lightweight nature and self-adhesiveness.

used with gold (Au) sputtering to construct conical microneedles for various biopotential measurements.[16]

Alternatively, to realize non-contact, capacitive ECG electrodes, aluminum conductive foil, and copper were used and dry electrodes were formed on polyimide substrates.[17] Another approach relied on simply attaching conductive textiles on dry polymer foams to realize a cloth-attachable and capacitive biopotential sensing monitor.[18] Copper/nickel-plated composition was also used to develop a capacitive infant underwear design.[19] Likewise, a three-electrode ECG t-shirt model with a built-in driven right leg electrode and two capacitive differential electrodes,[20] and a manually adjustable, pressure-sensitive capacitive belt design were proposed.[21] Despite the steady progress and various efforts to adjust the skin-electrode contact pressure,[22,23] capacitive electrodes inherently suffer from motion artifacts and display high skin-electrode impedance due to the inevitable gap between the sensing region and the skin surface or clothing.[24] On the other hand, due to their intrinsic mechanical properties, such as stretchability and elasticity, surface polymeric electrodes are also great alternatives for biopotential measurements. Poly(3,4-ethylene dioxythiophene): polystyrene sulfonate (PEDOT:PSS) and PDMS are used mostly in skin-like electronics.[25] Applications also include waterborne polyurethane (WPU) for improved stretchability as well as D-sorbitol for better adhesiveness and tolerance to motion artifacts.[26] Along the same lines, tattoo electrodes were proposed where conductive polymers were formed on commercial decal paper using inkjet printing,[27] and thin film metals were deposited on polyethylene terephthalate (PET) substrate.[28] Carbon nanofillers were also used to build micropillars to improve the attachment without penetrating the skin.[29,30]

More recently, to realize surface biopotential electrodes, carbon-based materials primarily graphene[31] has been proposed due to their intrinsic properties, such as electrical conductivity,[32] high stability, flexibility,[33] biocompatibility,[34] and mechanical durability.[35] Skin-compatible tattoos employing graphene were also developed.[36] to increase the signal-to-noise (SNR) ratio by excellent adhesion to the skin through self-adhesive materials[37] and Van der Waals forces.[38] Additionally, graphene-based wearable sensors have been developed for various applications, leveraging the exceptional material and mechanical properties of graphene. These applications include motion detection through skin strain monitoring[39,40] and thermometry for temperature measurement and proximity detection.[41]

To reduce graphene oxide (GO), typically toxic materials such as hydrazine and sodium borohydride have been widely utilized.[42] However, their potential toxicity must be carefully evaluated, especially for applications involving direct contact with the human body. As an eco-friendly alternative, L-ascorbic acid ($C_6H_8O_6$), commonly known as Vitamin C, has emerged as a "green reduction" agent offering several advantages. It is non-corrosive, non-carcinogenic, and non-toxic. Studies have highlighted its remarkable effectiveness in reducing GO.[43,44] Of particular importance are textile electrodes as they are naturally wearable, soft, and feasible to implement. Moreover, the mesh layout of the weaves in textiles makes them suitable for biopotential measurements on the skin as this structure can route the signal energy in the "*z*" direction; normal to the skin surface. This allows easy and robust electrical interfacing to the textile electrodes and therefore a stable skin-electrode contact that is free from potential disturbance due to sideway interconnects (e.g. with FPC cables and connectors) is achieved. In an effort to unite the favorable properties of graphene and textiles,

ordinary fabrics such as nylon, and cotton were functionalized by graphene through a straightforward dip-dry-reduce strategy, and wearable, soft graphene textile biopotential electrodes with excellent performance were realized.[45]

Among different materials used in synthesizing textile fibers such as polyester, nylon, cotton, and acrylic fabrics; acrylic fabrics have a spin-coatable and patternable form which is PMMA. The very availability of a spin-coatable and patternable PMMA opens up new venues to realize "textile-like" micro/nanostructured surfaces similar to weaved textiles which can be functionalized by dip-coating for instance with graphene. To pattern PMMA, electron beam lithography (EBL) is widely used and can directly write high-resolution patterns;[46] yet, EBL is a resource-intensive method requiring dedicated infrastructure and lengthy process cycles.[47]

In this work, we demonstrate a cost-effective, straightforward approach of utilizing $O_2$ plasma-based dry etching along with photolithography to selectively etch and structure the PMMA surface, much like a weft and warp pattern as shown in **Figure 1a**. This unique approach allowed us to "artificially-weave" the PMMA, and essentially realize a textile-like polymeric (TPM) surface. To render a mechanically robust TPM structure, a 50 µm-thick layer of SU-8 was used as the backing layer, which supported the relatively thin PMMA surface. Thereafter, the TPM surface could be functionalized by drop-casting GO and converting to reduced graphene oxide (rGO) using an environmentally-friendly vitamin C (L-ascorbic acid) reduction agent, effectively realizing flexible TPM electrodes for biosignal monitoring. We demonstrate the excellent performance of TPM electrodes in recording ECG signals alongside conventional Ag/AgCl electrode, where the TPM electrodes achieve a correlation score of 98.84%, and signal to noise ratio (SNR) of 28.26 dB which is very close to 28.3 dB achieved by conventional electrodes. Alongside their performance in biopotential recording, we demonstrate the superior mechanical properties of this new artificially-weaved TPM electrode, together with its attributes such as electrode flexibility, self-adhesive properties, ability to continuously record signals up to tens of minutes, and long-term stability even after immersion to water for 5 days.

## 2. Experimental Section

### 2.1. Fabrication of TPM Electrodes

#### *2.1.1. Deposition of $SiO_2$ Sacrificial Layer*

The process begins with depositing sacrificial material with a thickness of 500 nm on a Si wafer by using plasma-enhanced chemical vapor deposition (PECVD) (Oxford Plasmalab System 100). Silane ($SiH_4$) and nitrous oxide ($N_2O$) gases were used in PECVD to grow the $SiO_2$ film. $SiO_2$ layer served as a sacrificial layer to be etched fully at the end of the fabrication process and release the structure.

#### *2.1.2. Photo-Patterning of SU-8 Resist*

A 50 $\mu$m-thick SU-8 negative photoresist (Kayaku Advanced Materials, Westborough, MA, USA) with Young's modulus of 2 GPa was used as a backing and to provide mechanical stability, as PMMA alone is too thin. It was spin-coated at 3000 rpm for 30 s with an initial spread cycle of 10 s at 300 rpm, then soft-baked at 65 °C for 5 min and 95 °C for 15 min, followed by exposure with 365 nm UV light at a dose of 70 mJ $cm^{-2}$ for 9 s. Next, post-exposure bake for 2 min at 65 °C and 7 min at 95 °C, then 4 min development in SU-8 developer (i.e. 1-methoxy-2-propyl acetate).

#### *2.1.3. Photo-Patterning of Cu Hard Mask for PMMA Etching*

PMMA (495K MW PMMA-C4) was spin-coated on the patterned SU-8 surface at 4000 rpm for 45 s to reach 400 nm thickness. It was later baked at 180 °C for 10 min. 500 nm thick copper (Cu) was used as a protective layer which was thermally deposited (Nanovak R&D, Ankara, Turkey) at a chamber pressure of $10^{-6}$ Torr. Next, AZ5214 photoresist (PR) was spin-coated at 4000 rpm for 30 s to reach 1.2 µm of thickness. The sample was then baked for 60 s at 105 °C on a hot plate. After the second mask alignment, the sample was exposed with 365 nm UV light at a dose of 70 mJ $cm^{-2}$ followed by immersion in AZ-726 developer for 40 s. The sample was finally immersed in distilled water (DI water) and dried with pressurized $N_2$ gas. The Cu layer was utilized as a hard mask to protect the underlying PMMA during $O_2$ plasma exposure.

#### *2.1.4. Etching PMMA Layer*

The substrate was immersed for 30 s in Cu etchant mixture of acetic acid, hydrogen peroxide, and DI water with a ratio of (1:1:18). Next, to pattern the PMMA layer, $O_2$ plasma etching (Oxford Plasmalab System 100) was performed for sufficiently long (≈13 min) to remove the PMMA in regions unprotected by the Cu hardmask.

#### *2.1.5. Release SU-8/PMMA Composite "Weft-Warp" Structure*

To finalize the fabrication, the residual photoresist layer was stripped, and the Cu hard mask layer was removed using acetic acid and hydrogen peroxide solution. Then, the samples were immersed into buffered oxide etchant (BOE 7:1) (MicroChemicals GmbH, Ulm, Germany) for 5 h to remove the underlying silicon dioxide layer and release the SU-8/PMMA composite "weft-warp" structure that was surface-micromachined on the Si wafer. A 3D schematic of the fabrication process flow is shown in Figure 1a. Detailed microscope images illustrating the fabrication process are available in Figure S1 (Supporting Information).

#### *2.1.6. Electrode Preparation*

Graphene oxide (GO) was prepared using the modified Hummers method. The coating process includes drop-casting of diluted GO suspension on the SU-8/PMMA sample on a hydrophobic polytetrafluoroethylene (Teflon) surface. 0.3 ml GO was drop-casted, and the sample was left at room temperature for a day to allow the evaporation of the solvent. Many attempts have been

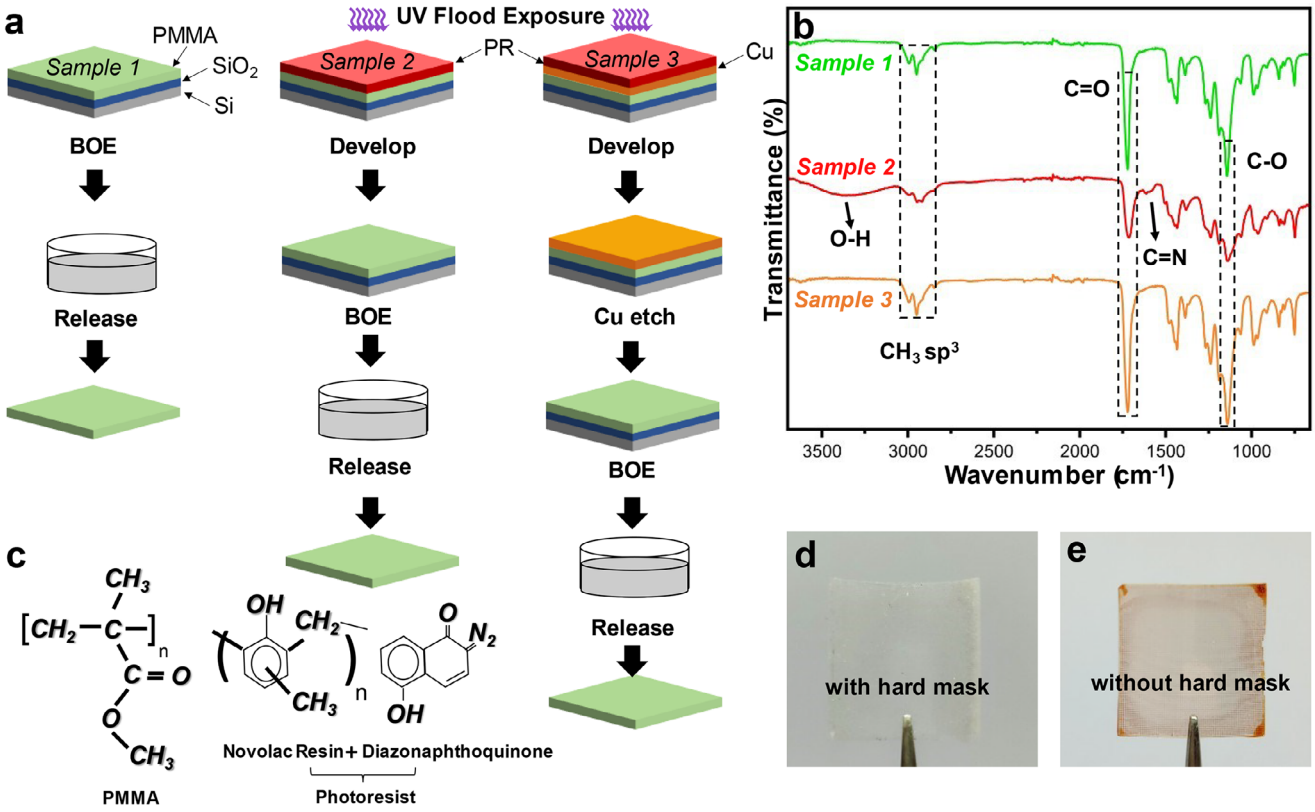


**Figure 2.** a) Fabrication process flow of three samples to evaluate the surface residues on PMMA with and without utilizing copper (Cu) as the hard mask; b) Fourier-transform infrared spectroscopy (FTIR) analysis for the three samples; c) chemical structure of PMMA and photoresist; and d,e) Images of 2 × 2 cm electrodes comparing the SU-8/PMMA substrate with and without using the hard mask technique.

made to reduce the GO-coated TPM substrate such as chemical reduction and thermal reduction. However, both methods yielded undesirable results (see Note S1, Supporting Information).

To address these issues an eco-friendlier option, i.e. vitamin C, was employed as a chemical-reducing agent. The reduction process includes preparing a solution of 0.35 g $ml^{-1}$ L-ascorbic acid and DI water by mildly stirring them for 15 min at room temperature, followed by immersing the GO-coated sample into the prepared solution for three days at room temperature. Then, the sample was cycled in DI water to rinse the residual vitamin C and left at room temperature for drying to realize the TPM electrode (Figure 1b). This allowed successful reduction of GO without delamination and at the same time ensured a high-quality surface finish. The final thickness of the electrode was between 85 and 95 µm. Furthermore, a 2 × 2 cm TPM electrode was weighed as 15.7 mg exhibiting a lightweight nature (Figure 1c).

### 2.2. Characterization of the TPM Electrode

The impact of using a hard mask on the underlying PMMA layer was evaluated through Fourier-transform infrared spectroscopy (FTIR) (Nicolet iS10, Thermo Fisher Scientific). For this experiment, three samples with the following multi-layer stack topologies were prepared: 1) $Si/SiO_2/PMMA$, 2) $Si/SiO_2/PMMA/PR$, and 3) $Si/SiO_2/PMMA/Cu/PR$. First, the PR layer was removed from the second and third samples by UV flood exposure and development in AZ 726 MIF (Merck, Darmstadt, Germany) (**Figure 2a**). Next, the copper layer was etched from the third sample by a mixture of acetic acid, hydrogen peroxide, and DI water with a ratio of (1:1:18). Finally, the three samples were released using BOE for 12 h to obtain structurally intact layers of PMMA.

In the first sample consisting of pure PMMA, the FTIR spectrum (Figure 2b) confirms the presence of the ester C═O bond ≈1720 $cm^{-1}$, and the band between 1120 and 1220 $cm^{-1}$ attributed to C—O stretching vibration. Likewise, two small peaks located in the 3000 to 2900 $cm^{-1}$ band of the PMMA spectra are assigned to —CH $sp^3$, which are also in alignment with the previously published data.[48,49] We can observe the same peaks in the third sample's infrared spectra, which was prepared using the hard mask technique. This observation confirms that the hard mask (copper) does not leave any residues or affect the composition of PMMA afterward. However, the spectrum of the second sample reveals both the characteristic peaks of pristine PMMA, along with a peak ≈3350 $cm^{-1}$ indicating O—H stretch due to Novolak resin; as well as, peaks between 1650 and 1550 $cm^{-1}$, confirming C═N stretching from naphthoquinone diazide, both of which hint at the chemical structure of photoresist.[50,51] (Figure 2c). This result confirms that using a photoresist as an etch mask to pattern PMMA is likely to leave hardened surface residues as evidenced by the identified peaks associated with the novolak resin and naphthoquinone diazide. The existence of photoresist residues on PMMA surface is also visible by the reddish color of the sample prepared without the Cu hard

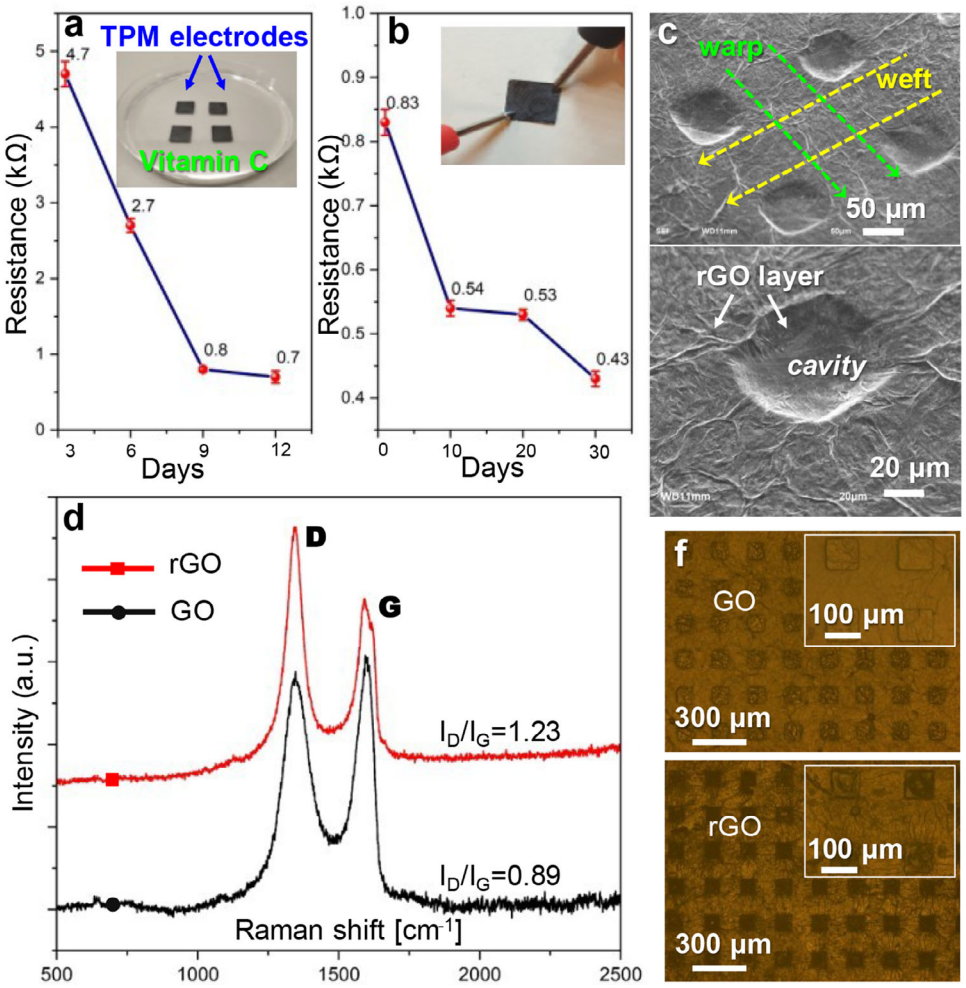


**Figure 3.** a) Resistance measurement of TPM electrode immersed in vitamin C solution for 3, 6, 9, 12 days, respectively; b) monitoring the stability of TPM electrode resistance over a month period for an electrode that was initially reduced in vitamin C solution for 9 days; c) Scanning electron microscopy images (SEM) of the TPM electrodes; d) Raman spectra of graphene oxide (GO) and reduced graphene oxide (rGO) traces; f) Optical microscope images of TPM electrode before and after GO reduction.

mask (Figure 2d,e). Furthermore, the UV light protective effect of the Cu layer on PMMA was evaluated using FTIR analysis. A $Si/SiO_2$/PMMA/Cu multilayer was fabricated, and the sample was exposed to 365 nm UV light at a dose of 70 mJ $cm^{-2}$. Subsequently, the Cu layer was removed using the Cu etchant, the $SiO_2$ layer was etched, and the PMMA layer was released. FTIR analysis of the released PMMA layer revealed the same characteristic PMMA peaks as discussed earlier, demonstrating the high level of protection provided by the Cu layer (data available in Figure S2, Supporting Information).

The resistance of the TPM electrode after 3 days of immersion in the reduction solution was 4.7 kΩ. Therefore, To evaluate the impact of immersion duration on the quality and degree of reduction of GO using vitamin C, a 2 × 2 cm TPM substrate was coated with GO and allowed to dry for one day. The dried substrate was then cut into four pieces, each measuring 1 × 1 cm, and soaked in the vitamin C solution. Every three days, a sample was removed from the solution and allowed to dry in ambient air for 24 h before measuring its resistance. This process was repeated for all four samples, with the first sample being immersed for three days and the fourth sample immersed continuously for a total of twelve days. As shown in **Figure** 3a, the resistance values measured after immersion were 4.7 kΩ after three days, 2.7 kΩ after six days, 0.83 kΩ after nine days, and 0.67 kΩ after twelve days. With respect to electrode resistance after the initial 3 days of reduction, the resistance drops were ≈42.5%, 69.3%, and 19.2% in each consecutive 3-day intervals (i.e. after a total of 6, 9, and 12 days of reduction, respectively). These results show that TPM electrode's resistance falls significantly within 9 days of immersion in the reduction solution, and stabilizes within 12 days. Therefore, to achieve a resistance below 1 kΩ for the GO film, 9 days was selected as the optimal duration in the vitamin C solution. Further, after selecting the optimal duration, the resistance of the electrode was measured every 10 days for one month. The electrode resistance displayed a decreasing trend from 0.83 to 0.43 kΩ in one month (Figure 3b); with a rapid fall during the first 10 days and remaining relatively stable thereafter. This decreasing trend in resistance is likely attributed to the gradual removal of oxygen functional groups from the rGO layer as time passes at room temperature.

Scanning electron microscopy (SEM) imaging of the TPM electrode was performed to inspect the conformality of the rGO coating on the "artificially-weaved" microstructured PMMA surface (Figure 3c). The images verify that the gaps between stripes are well-filled with rGO homogenously, effectively providing an electrical connection between the top and bottom faces of the electrode. This is advantageous to realize a reliable skin-electrode contact and highly feasible for electrical wiring purposes, facilitating the acquisition of biopotential signals without disturbing the skin-electrode contact. Furthermore, the "weft-warp"-like microstructured surface also promotes the conformal layering of GO onto the SU-8/PMMA substrate, and thereafter, upon GO reduction, helps preserve the rGO coating. The attachment of the graphene oxide to the substrate can be attributed to two primary mechanisms: chemical interactions and mechanical interlocking. At the GO-polymer interface, van der Waals forces and hydrogen bonding play a key role in promoting adhesion. These interactions occur naturally due to the functional groups present on the GO surface and the substrate.[52,53] Along with the surface interactions, the microscale periodically-textured surface of the SU-8/PMMA substrate, featuring an array of 100 µm square gaps, further enhances the GO adhesion. This structuring allows GO to conform to the substrate's contours, effectively creating a GO film comprising a network of interconnections extending both in planar and out-of-plane directions (Figure S3, Supporting Information). On the other hand, without the microstructured surface, the rGO layer detaches from unpatterned, smooth SU-8/PMMA surfaces upon reduction and sample rinse (Figure S4, Supporting Information). This highlights the importance of the "weft-warp" pattern in stabilizing the layering and attachment of rGO onto the SU-8/PMMA polymer composite substrate.

To confirm the transition of GO to rGO by the reduction agent (ascorbic acid), Raman spectroscopy (Renishaw, Wotton-under-Edge, UK) was performed with a 532 nm excitation laser and 1 $cm^{-1}$ spectral resolution. Raman shifts of graphene-based materials show two peaks referred to as the D and G bands, varying from 1308 to 1375 $cm^{-1}$ for GO and 1536 to 1599 $cm^{-1}$ for rGO. The G-band is commonly associated with the presence of C—C bond in $sp^2$ of carbon atoms in the 2D hexagonal plane. As a result, the ratio of the D and G band intensities ($I_D/I_G$) illustrates the reduction extent that results from the restoration of graphene structure and the removal of oxygen atoms from GO. As shown in Figure 3d, while the $I_D/I_G$ ratio for GO is 0.89, it increases to 1.23 after the reduction process with ascorbic acid. This confirms the reduction of GO to rGO and restoration of graphene structure due to the removal of oxygen atoms from GO. Figure 3f shows that the GO-coated surface preserves uniformity after the reduction process.

### 2.3. Skin-Electrode Impedance

A measurement circuit based on a previously developed design [45,54] was built to find the impedance of TPM electrodes and to compare it with commercial Ag/AgCl electrodes. The experiment setup is described in Note S2 (Supporting Information). As shown in **Figure 4** the impedance of the Ag/AgCl varies between 20.83 and 5.42 kΩ, respectively. On the other hand, TPM electrodes vary in the range of 35.56 and 7.83 kΩ. Although there is a slight difference in impedance values, such differences are not critical and the skin-electrode impedance of the electrodes is still well within the range of contact impedance values necessary for high-performance biopotential recordings.

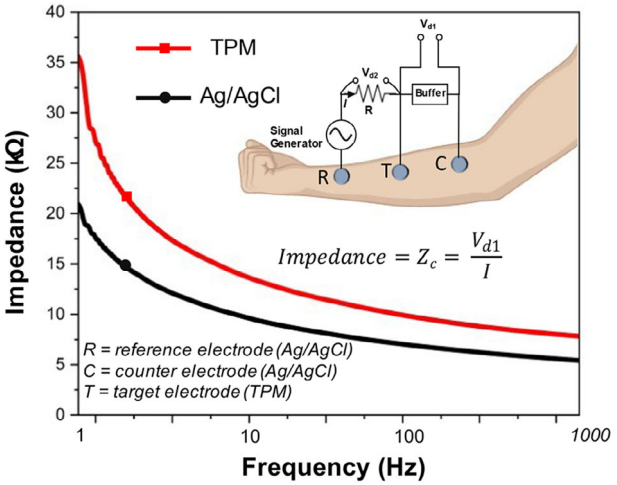


**Figure 4.** Skin-electrode contact impedance in relation to frequency variation with the inset of the experimental setup for the TPM and Ag/AgCl electrodes.

## 3. Results and Discussion

### 3.1. ECG Signal Recording

The wiring setup of TPM electrode and ECG signal filtering process are described in detail in Notes S3 and S4 (Supporting Information). **Figure 5a** shows an exploded view of the electrode topology consisting of different layers, along with images of a fabricated electrode placed on the upper arm.

The first experiment series was performed on a 32-year-old participant with no known cardiovascular disease history. The participant was instructed to sit still under static conditions on a chair in front of the data collection setup. TPM electrodes were placed in lead-I configuration, and they were fixated on the arm by applying a drop of water to humidify the skin and thereafter relying on the self-adhesive ability of the electrodes without using any extra materials. The self-adhesive nature of TPM electrodes is attributed to Van der Waals interactions and contact electrification[38,55] which are likely supplemented by capillary forces due to interfacial humidity [56] and augmented by the ultrathin electrode body and the concave geometry of micromachined cavities.[57] The self-adhesiveness of 2 × 2 cm TPM electrodes even under conditions of excessive movements (Movie S1, Supporting Information) along with their capability to acquire ECG signals in real-time during severe hand movements (Movie S2, Supporting Information). Additionally, the long-term stability of the TPM electrode was evaluated by recording ECG signals before and after six months of storage in ambient air. The SNR was calculated for both recordings showing a nearly unchanged value (Figure S5, Supporting Information), which indicates stable electrode performance and reliable functionality even after an extended period.

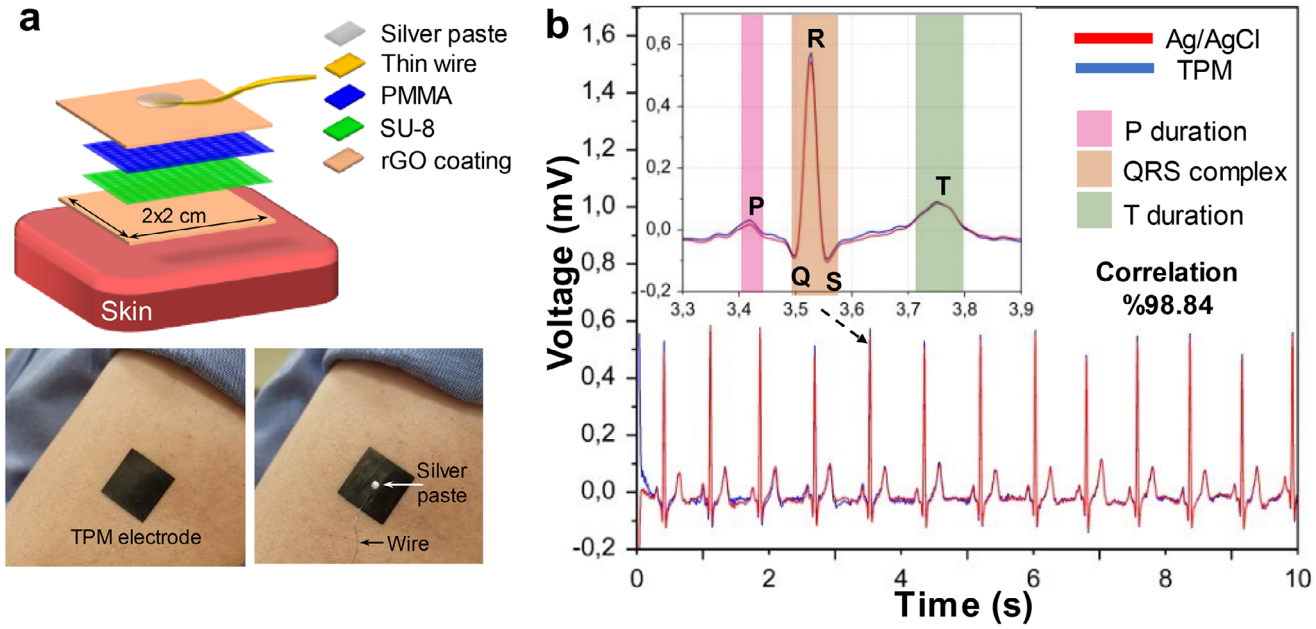


**Figure 5.** a) Exploded view of a TPM electrode showing its inner layers with images of 2 × 2 cm electrode placed on the upper arm with and without wiring, b) Simultaneous ECG recording with TPM and Ag/AgCl electrodes.

As the electrode position highly affects the signal morphology, wet Ag/AgCl electrodes were placed right next to the TPMs to make a fair comparison between the two. The PQRST complex was clearly visible in the collected datasets. Figure 5b shows almost two identical ECG traces recorded with the TPM and Ag/AgCl electrodes that exhibit a correlation of %98.84. The signals showed SNR scores of 28.26 and 28.3 dB, and RMS noise of 18.4 and 17.75 μV, for the TPM and Ag/AgCl electrodes; respectively.

The second series of experiments were performed to assess the electrode's self-adhesive ability in long-term ECG recording (i.e., 30 min). No adhesive materials were used to observe the self-adhesiveness of TPM electrodes. The participant was again instructed to sit down in front of a monitor, and the data was collected while he was watching a half-hour-long TV series episode in his preference, where he occasionally twitched his arms voluntarily to relieve his arm muscles. Ag/AgCl electrodes were placed next to TPM electrodes on both upper arms to perform synchronous data acquisition.

In **Figure** 6a five-second temporal windows, extracted from the 30 min-long electrocardiogram recording, at every 6 min intervals and its multiples are shown. SNR scores of TPM electrodes are higher signal in all of the five signal segments of up to 0.7 dB. The mean RMS noise changed from 41.92 to 46.6 μV, and SNR changed from 21.06 to 26.17 dB for the TPM electrodes; while Ag/AgCl displayed mean RMS noise from 43.41 to 47.8 μV and SNR changed from 20.81 to 25.88 dB (Figure 6b). The relative standard deviation (RSD) is calculated as %4, which demonstrates the outstanding stability of the TPM electrodes even in long ECG recordings.

To investigate the waterproof surface of the TPM electrodes they were kept immersed in water for five days. Each day, they were used to collect data from the same participant, and the signal was observed to see if the electrodes were degraded. Figure 6c shows these ECG recordings acquired with the TPM electrode for 6 consecutive days, where the electrode was kept immersed in water for 5 days. The SNR score before wet immersion was calculated as 15.94 dB. Then from the first day to the last the SNR dropped from 17.92 to 16.029 dB with relative standard deviation of 15%, where we attribute to experimental measurements errors. The RMS noise before immersion was calculated as 43.82 μV, and then from first day to the last it ranged from 44.79 to 47.087 μV with a relative standard deviation of %9.1 (Figure 6d). The stability of the SNR and mean RMS noise scores verifies the functionality of TPM electrodes in wet environments and proves their durability.

Moreover, the electrode retains its performance in highly humid environments, preserving the clarity and integrity of the PQRST segments of the ECG signal (Movie S3, Supporting Information). Additionally, the electrode's robustness was evaluated under varying pH conditions, including a pH 4 acidic solution and a pH 8 basic solution. It maintained consistent performance across these pH levels, showing no significant change in sheet resistance, as illustrated in Figure S6 (Supporting Information).

Finally, the third series of experiments were conducted to assess the electrodes' water resistance capability in wet environments (e.g., perspiration during intense exercise). First the sessile drop method is used to determine the contact angle and verify the waterproof ability of the electrodes, where contact angles above 90° indicate that a sample is hydrophobic and therefore waterproof.[58] In this study (Theta Lite optical tensiometer) with a video-camera system and computer software was used to measure the static contact angle. Accordingly, a drop of water was applied onto the TPM electrode surface and then the contact angle was measured in the first 10 s after a droplet was formed on the surface. TPM electrodes on average showed a contact angle of 71° between the drop and the electrode surface (Figure 6e). The partially hydrophobic surface of the TPM electrode with of

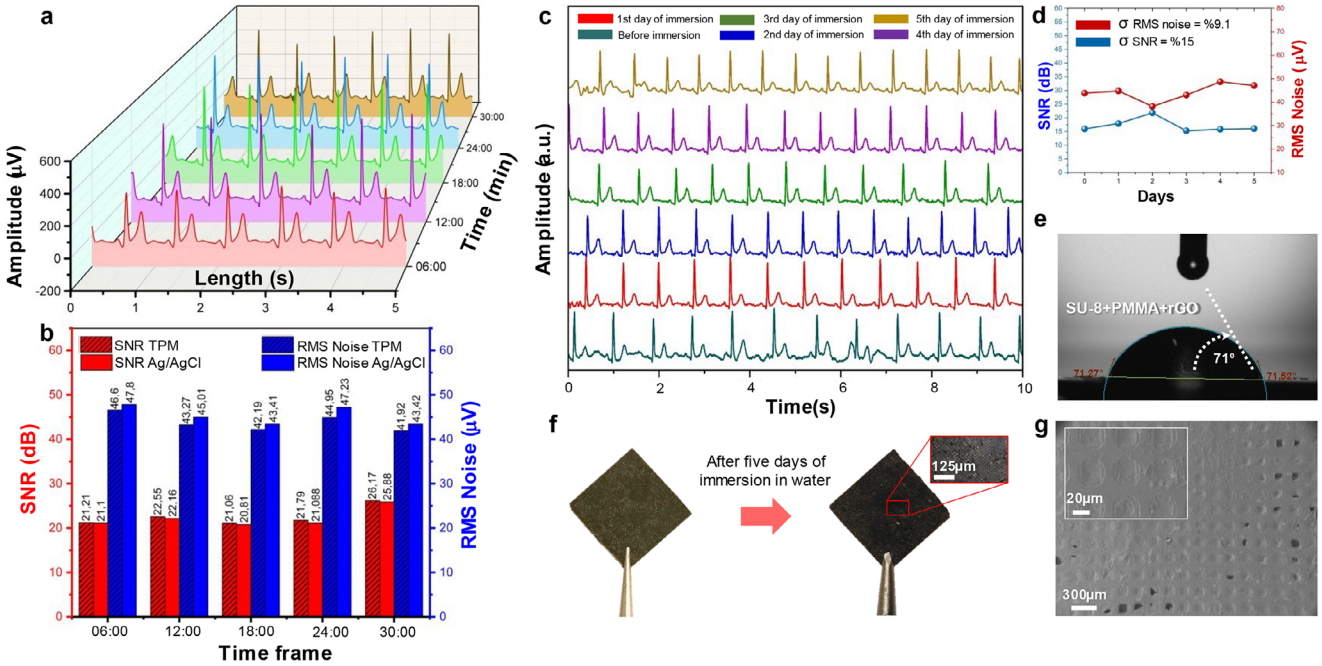


**Figure 6.** a) ECG acquisition for 30 min simultaneously for TPM and Ag/AgCl electrodes; b) signal-to-noise ratio and RMS noise for the five signal segments of the 30 min-long ECG; c) waterproof capability of TPM electrodes are demonstrated by consecutive ECG recordings of 10 s each during 5 days of immersion into water; d) signal-to-noise ratio and RMS noise of the ECG signal taken before and during a 5-day period with the TPM water-immersed electrodes; e) contact angle of the TPM electrode; f) photos of 2 × 2 cm TPM electrode in dry state and after immersing the electrodes into the electrodes inside water for 5 days; g) SEM image of the TPM electrode after remaining in water for 5 days.

71° contact angle allows it to display some waterproof capability. Photos of the electrode before and after five days of constant water immersion show minimum visual deformation on the rGO surface (Figure 6f). SEM images of the surface after five days of water immersion indicate only small deformations occurring on the surface as empty spots (Figure 6g).

Additionally, the 5-day ECG acquisition using TPM electrodes immersed in water reveals that the presence of empty spots on the electrode doesn't result in any signal disturbances, which assures the reusability of the TPM electrode under intense wet conditions.

### 3.2. Bending Experiment, Sheet Resistance, and Tensile Test

Several experiments were performed to evaluate the mechanical and electrical stability of the electrode even in harsh continuous use conditions. First, a manual where they undergo a gradual force applied by compressing an electrode initially aligned parallel to the vertical direction with two fingers (**Figure** 7a) which is detailed in Note S5, and Figure S7 (Supporting Information). Then we have also verified the performance of the electrodes in cyclic operation where they were subjected to successive bending cycles to observe the effects of mechanical deformations on the physical surface. The experiment was performed by placing the TPM electrode on polyethylene terephthalate (PET) film and fixing it on a voice coil actuator which can be driven with different waveforms to adjust the bending angle during repetitive compression as shown in Figure 7b. SEM images were obtained in each phase to assess the degradation level on the rGO surface after each experimental cycle, which shows that there is not much change (Figure 7c). Likewise, the change of electrode sheet resistance (Rs) with respect to bending was quantified with a four-point probe unit (C4S, Cascade Microtech, Beaverton, Oregon, US) before and after bending up to 200 cycles. The baseline Rs prior to bending was measured as 103 Ω $sq^{-1}$. which increased to ~179 Ω $sq^{-1}$, after 4 bending cycles with 200 repetitions of compression up to 45° **Table** 1, summarizes the change of $R_s$ with bending cycle.

Despite the increasing trend in sheet resistance, the SEM images revealed no visible damage on the rGO surface after 100 bending and a very subtle change in rGO surface after 200 bending cycles. The stability of the electrode was further demonstrated by successfully recording ECG signals after 200 bending cycles (Figure S8, Supporting Information).

Further, to evaluate the effect of the PMMA layer on the mechanical properties of the SU-8 substrate, a tensile test was performed, and the experiment setup is detailed in Note S6 (Supporting Information). Movie S4 (Supporting Information) demonstrates the sample and the data acquired during the tensile test. The results revealed a slight change in the Young's modulus from 1.8 ± 0.81 GPa to 1.9 ± 0.32 GPa after the inclusion of the PMMA layer. The measured Young's modulus is slightly different from the SU-8 manufacture datasheet value of (2 GPa), which is attributed to fabrication conditions such as UV exposure time and temperature,[59,60]

To assess the mechanical prosperities of the SU-8 substrate before and after adding the PMMA layer, toughness is calculated by the area under the stress–strain graph. The results offered an increase from 0.47 ± 0.036 to 0.98 ± 0.15 MJ $m^{-3}$ which is a

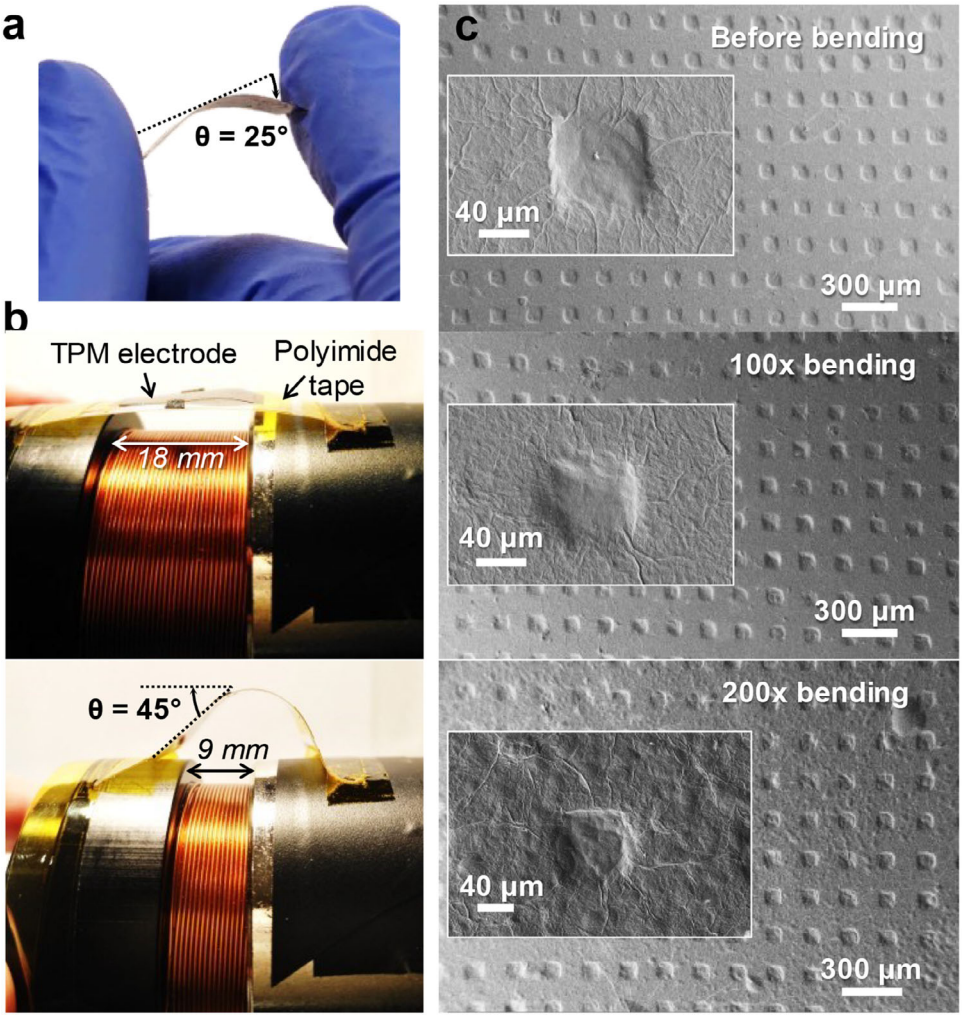


**Figure 7.** a) Bending test setup, b) SEM images of the electrode before the bending, after 100, and after 200 times bending applied.

significant increase of 108.5% in the SU-8/PMMA substrate toughness. The toughness represents the amount of energy the sample can bear before fracture.[61] Thus, the new composite can withstand more load before it fails, indicating enhancement of the mechanical properties after adding the PMMA layer. Likewise, the strain and ultimate strength of the SU-8/PMMA composite showed an increase of 66.7% and 37.7%, respectively. **Table 2** summarizes the SU-8 and SU-8/PMMA mechanical properties.

Based on the measurement results, the most robust electrode is SU-8/PMMA composite TPM, where the thin layer of PMMA makes the electrode more robust, leading to a lower risk of breaking. Even though the PMMA layer thickness is 300 nm, the effect of the acrylic-based flexible PMMA is dominant here. Adding the PMMA layer makes the electrode use repeatable and shows a promising result for wearable ECG monitoring.

## 4. Conclusion

Inspired by graphene-textile electrodes we developed flexible artificial, textile-like polymer-based microstructured (TPM) electrodes with rGO functional layers. We demonstrate the self-adhesive, flexible, and water-proof nature of TPMs that render them suitable for wearable, long-term biopotential monitoring, specifically for electrocardiography (ECG). Poly (methyl methacrylate) (PMMA), a widely used polymer in the textile industry, and SU-8, a negative photoresist polymer, were used as the core materials and underwent microfabrication steps to achieve a textile-like structure of 100 µm gaps and 100 µm spacings resembling a "weft-warp" pattern. The unique textile-like microstructured electrodes could be conformally layered with rGO, both in-plane and vertical to the electrode surface

**Table 1.** Change of sheet resistance ($R_s$) with bending.

| Cycle count | Sheet resistance [$R_s$] ($\Omega$ sq$^{-1}$) | $\Delta R/R$ (%) |
|---|---|---|
| 0 | 103.51 ± 3.87 | 0 |
| 50 | 118.91 ± 11.128 | 14.88 |
| 100 | 132.61 ± 8.35 | 28.11 |
| 150 | 158.55 ± 12.4 | 53.17 |
| 200 | 178.94 ± 31.68 | 72.87 |

**Table 2.** Summary of the mechanical properties of SU-8 and SU-8/PMMA composite.

| Mechanical properties | SU-8 | SU-8/PMMA | % Δ |
|---|---|---|---|
| Young's modulus (GPa) | 1.8 ± 0.81 | 1.9 ± 0.32 | 5.5 |
| Strain | 0.024 ± 0.0022 | 0.04 ± 0.0066 | 66.7 |
| Ultimate strength (MPa) | 40.41 ± 1.14 | 55.63 ± 6.74 | 37.7 |
| Toughness (MJ $m^{-3}$) | 0.47 ± 0.036 | 0.98 ± 0.15 | 108.5 |

without compromising from the flexibility and self-adhesive nature of the electrode; while providing stable skin-electrode contact and electrical interfacing. The advantageous features and performance of TPMs are extensively characterized by "adhesive-free" and "elastic-band-free" repeatable acquisition of ECG signals; both in dry and wet environments, for durations reaching up to 30 min even under severe motion or flexural pre-stressing up to 200 bending cycles. The multiple unique advantages of TPM electrodes, along with the cost-effective, recyclable nature of graphene materials compatible with scalable manufacturing approaches, will be instrumental for wearable long-term biosignals monitoring reaching clinical-grade performance.

## 5. Statistical Analysis

The recorded ECG data was processed and filtered using custom-written MATLAB scripts. A notch filter was first applied to eliminate the powerline interference at 50 and 100 Hz. Then a band-pass filter was applied to remove noise outside the frequency range of 5 Hz to 50 Hz. Lastly, a fifth order moving average filter was applied to smooth the signal. The built-in correlation function in MATLAB was applied for 10 s of data to assess the similarity between simultaneously recorded ECG signals from Ag/AgCl and TPM electrodes. To assess the signal quality, signal-to-noise ratio (SNR) and RMS noise scores were calculated. Energy around the QRS complex was attributed as the "signal", while the remaining baseline fluctuations including the is potential line were considered as "noise" following the equation below.

$$SNR\,[dB] = 20\log\left(\frac{|E_{RRS}|}{E_{noise}}\right) \quad (1)$$

## Supporting Information

Supporting Information is available from the Wiley Online Library or from the author.

## Acknowledgements

This work was supported in part by Sabanci University. Professor Murat Kaya Yapici appreciates the support of the Turkish Academy of Sciences (TUBA) within the framework of the TUBA Outstanding Young Scientist Award Program (GEBIP'21); the Science Academy for the Young Scientist Award Program (BAGEP'23); and Elginkan Vakfi for the Technology Prize'24. The experimental procedures involving volunteer human subjects described in this research are followed by the ethical principles outlined in the Helsinki Declaration of 1964, as revised in 2013 and approved by the Ethics Committee of Sabanci University (FENS-2020-48). The participants provided their informed consent for inclusion before they participated in the study.

## Conflict of Interest

The authors declare no conflict of interest.

## Data Availability Statement

The data that support the findings of this study are available from the corresponding author upon reasonable request.

## Keywords

electrocardiography (ECG) monitoring, flexible electrode, graphene, polymethyl methacrylate (PMMA) e-beam resist, SU-8 photoresist, wearable bioelectrode, weft-warp micropattern

Received: December 2, 2024
Revised: January 27, 2025
Published online: April 5, 2025

[1] P. Karthikeyan, M. Murugappan, S. Yaacob, *J. Mech. Med. Biol.* **2013**, *13*, 1350038.
[2] F. Agrafioti, D. Hatzinakos, A. K. Anderson, *IEEE Trans. Affect. Comput.* **2012**, *3*, 102.
[3] S. Savonitto, *JAMA, J. Am. Med. Assoc.* **1999**, *281*, 707.
[4] P. J. Zimetbaum, M. E. Josephson, *N. Engl. J. Med.* **2003**, *348*, 933.
[5] J. W. Mason, *N. Engl. J. Med.* **1993**, *329*, 445.
[6] L. McNichol, C. Lund, T. Rosen, M. Gray, *J. Wound, Ostomy & Continence Nurs.* **2013**, *40*, 365.
[7] N. Meziane, J. G. Webster, M. Attari, A. J. Nimunkar, *Physiol. Meas.* **2013**, *34*, R47.
[8] D. Huang, J. Li, T. Li, Z. Wang, Q. Wang, Z. Li, *J. Micromech. Microeng.* **2021**, *31*, 073001.
[9] S. M. Lee, K. S. Sim, K. K. Kim, Y. G. Lim, K. S. Park, *Med. Biol. Eng. Comput.* **2010**, *48*, 447.
[10] S. S. Mirbakht, A. Golparvar, M. Umar, B. A. Kuzubasoglu, F. S. Irani, M. K. Yapici, *Adv. Sci.* **2025**, *12*, 2405988.
[11] A. Gowda, B. Healey, H. Ezaldein, M. Merati, *J. Clin. Aesthet. Dermatol.* **2021**, *14*, 45.
[12] H. Zhang, W. Pei, Y. Chen, X. Guo, X. Wu, X. Yang, H. Chen, *IEEE Trans. Biomed. Eng.* **2016**, *63*, 1136.
[13] M. Matteucci, R. Carabalona, M. Casella, E. Di Fabrizio, F. Gramatica, M. Di Rienzo, E. Snidero, L. Gavioli, M. Sancrotti, *Microelectron. Eng.* **2007**, *84*, 1737.
[14] M. Arai, Y. Nishinaka, N. Miki, *Jpn. J. Appl. Phys.* **2015**, *54*, 06FP14.
[15] L. Ren, S. Xu, J. Gao, Z. Lin, Z. Chen, B. Liu, L. Liang, L. Jiang, *Sensors* **2018**, *18*, 1191.
[16] A. K. Srivastava, B. Bhartia, K. Mukhopadhyay, A. Sharma, *Sens. Actuators, A* **2015**, *236*, 164.
[17] Y. Gao, V. V. Soman, J. P. Lombardi, P. P. Rajbhandari, T. P. Dhakal, D. G. Wilson, M. D. Poliks, K. Ghose, J. N. Turner, Z. Jin, *IEEE Trans. Instrum. Meas.* **2020**, *69*, 4314.
[18] T.-W. Wang, H. Zhang, S.-F. Lin, *IEEE Sens. J.* **2020**, *20*, 9265.
[19] T. Kato, A. Ueno, S. Kataoka, H. Hoshino, Y. Ishiyama, in *2006 Int. Conf. of the IEEE Engineering in Medicine and Biology Society*, IEEE, New York, NY **2006**, pp. 916.

[20] A. Zompanti, A. Sabatini, S. Grasso, G. Pennazza, G. Ferri, G. Barile, M. Chello, M. Lusini, M. Santonico, *Sensors* **2021**, *21*, 2777.
[21] A. Alam, A. Q. Ansari, S. Urooj, in *2022 IEEE Delhi Section Conference (DELCON)*, IEEE, New Delhi, India **2022**, pp. 1–4.
[22] J. Lee, J. Heo, W. Lee, Y. Lim, Y. Kim, K. Park, *Sensors* **2014**, *14*, 14732.
[23] D. U. Uguz, Z. T. Canbaz, C. H. Antink, M. Luken, S. Leonhardt, *IEEE Trans. Instrum. Meas.* **2022**, *71*, 1.
[24] H. Ullah, M. A. Wahab, G. Will, M. R. Karim, T. Pan, M. Gao, D. Lai, Y. Lin, M. H. Miraz, *Biosensors* **2022**, *12*, 630.
[25] G. Li, Z. Qiu, Y. Wang, Y. Hong, Y. Wan, J. Zhang, J. Yang, Z. Wu, W. Hong, C. F. Guo, *ACS Appl. Mater. Interfaces.* **2019**, *11*, 10373.
[26] L. Zhang, K. S. Kumar, H. He, C. J. Cai, X. He, H. Gao, S. Yue, C. Li, R. C.-S. Seet, H. Ren, J. Ouyang, *Nat. Commun.* **2020**, *11*, 4683.
[27] L. M. Ferrari, S. Sudha, S. Tarantino, R. Esposti, F. Bolzoni, P. Cavallari, C. Cipriani, I. Mattoli, F. Greco, *Adv. Sci.* **2018**, *5*, 1700771.
[28] Y. Wang, Y. Qiu, S. K. Ameri, H. Jang, Z. Dai, Y. Huang, N. Lu, *npj Flexible Electron.* **2018**, *2*, 1.
[29] H.-L. Peng, J.-Q. Liu, H.-C. Tian, B. Xu, Y.-Z. Dong, B. Yang, X. Chen, C.-S. Yang, *Sens. Actuators, A* **2015**, *235*, 48.
[30] T. Kim, J. Park, J. Sohn, D. Cho, S. Jeon, *ACS Nano* **2016**, *10*, 4770.
[31] S. N. Alhasan, S. S. Mirbakht, S. Guler, O. Sahin, M. Umar, B. A. Kuzubasoglu, M. K. Yapici, in *Proc. Eurosensors Conf*, **2024**, pp. 181–182.
[32] M.-S. Cao, X.-X. Wang, W.-Q. Cao, J. Yuan, *J. Mater. Chem. C* **2015**, *3*, 6589.
[33] J. Yang, P. Hu, G. Yu, *APL Mater.* **2019**, *7*, 020901.
[34] J. Yang, K. Zhang, J. Yu, S. Zhang, L. He, S. Wu, C. Liu, Y. Deng, *Adv. Mater. Technol.* **2021**, *6*, 2100262.
[35] D. G. Papageorgiou, I. A. Kinloch, R. J. Young, *Prog. Mater. Sci.* **2017**, *90*, 75.
[36] S. Kabiri Ameri, R. Ho, H. Jang, L. Tao, Y. Wang, L. Wang, D. M. Schnyer, D. Akinwande, N. Lu, *ACS Nano* **2017**, *11*, 7634.
[37] L. Zhang, K. S. Kumar, H. He, C. J. Cai, X. He, H. Gao, S. Yue, C. Li, R. C. S. Seet, H. Ren, J. Ouyang, *Nat. Commun.* **2020**, *11*, 4683.
[38] D.-H. Kim, N. Lu, R. Ma, Y.-S. Kim, R.-H. Kim, S. Wang, J. Wu, S. M. Won, H. Tao, A. Islam, K. J. Yu, T. Kim, R. Chowdhury, M. Ying, L. Xu, M. Li, H.-J. Chung, H. Keum, M. McCormick, J. A Rogers, *Science* **2011**, *333*, 838.
[39] K. Manna, L. Wang, K. J. Loh, W. Chiang, *Adv. Mater. Interfaces* **2019**, *6*, 1900034.
[40] Y. Lin, Y. Zhao, L. Wang, Y. Park, Y. Yeh, W. Chiang, K. J. Loh, *Adv. Mater. Technol.* **2020**, *6*, 202000861.
[41] M. Umar, F. S. Irani, S. S. Mirbakht, M. K. Yapici, *Adv. Electron. Mater.* **2024**, *10*, 2300723.
[42] I. O. Faniyi, O. Fasakin, B. Olofinjana, A. S. Adekunle, T. V. Oluwasusi, M. A. Eleruja, E. O. Ajayi, *SN Appl. Sci.* **2019**, *1*, 1181.
[43] M. J. Fernández-Merino, L. Guardia, J. I. Paredes, S. Villar-Rodil, P. Solís-Fernández, A. Martínez-Alonso, J. M. Tascón, *J. Phys. Chem. C* **2010**, *114*, 6426.
[44] M. T. Aunkor, I. M. Mahbubul, R. Saidur, H. S. Metselaar, *RSC Adv.* **2016**, *6*, 27807.
[45] M. K. Yapici, T. Alkhidir, Y. A. Samad, K. Liao, *Sens. Actuators, B* **2015**, *221*, 1469.
[46] A. A. Tseng, K. Chen, C. D. Chen, K. J. Ma, *IEEE Trans. Electron. Packag. Manuf.* **2003**, *26*, 141.
[47] P. W. Doll, A. Al-Ahmad, A. Bacher, A. Muslija, R. Thelen, L. Hahn, R. Ahrens, B. Spindler, A. E. Guber, *Mater. Res. Express* **2019**, *6*, 065402.
[48] R. Huszank, E. Szilágyi, Z. Szoboszlai, Z. Szikszai, *Nucl. Instrum. Methods Phys. Res., Sect. B* **2019**, *450*, 364.
[49] N. D. Singho, N. A. Lah, M. R. Johan, R. Ahmad, *Int. J. Electrochem. Sci.* **2012**, *7*, 5596.
[50] R. Andok, A. Benčurová, P. Nemec, A. Konečníková, L. Matay, J. Škriniarová, P. Hrkút, *J. Electr. Eng.* **2013**, *64*, 371.
[51] S. Rimal, S. Koskey, T. Mukherjee, A. Goswami, J. Abdelghani, N. Ross, O. Chyan, in *Proc. SEMICON Korea, Seoul, Korea*, **2012**.
[52] J. Y. Choi, X. Zhang, H. T. Nguyen, M. R. Roenbeck, L. Mao, R. Soler-Crespo, S. T. Nguyen, H. D. Espinosa, *J. Mech. Phys. Solids* **2021**, *156*, 104578.
[53] Q.-Q. Huang, Y.-E. Wen, H. Bai, Z. Zhang, Y. Jiang, *Langmuir* **2021**, *37*, 8829.
[54] M. S. Spach, R. C. Barr, J. W. Havstad, E. C. Long, *Circulation* **1966**, *34*, 649.
[55] H. Izadi, A. Penlidis, *Macromol. React. Eng.* **2013**, *7*, 588.
[56] F. W. DelRio, M. P. de Boer, L. M. Phinney, C. J. Bourdon, M. L. Dunn, *Proceedings of the ASME 2006 Int. Mechanical Engineering Congress and Exposition*, The American Society of Mechanical Engineers, Chicago, Illinois **2006**.
[57] S. Chun, D. W. Kim, S. Baik, H. J. Lee, J. H. Lee, S. H. Bhang, C. Pang, *Adv. Funct. Mater.* **2018**, *28*, 1805224.
[58] T. M. Abbas, S. I. Hussein, *J. Inorg. Organomet. Polym. Mater.* **2022**, *32*, 3788.
[59] H. Yu, O. Balogun, B. Li, T. W. Murray, X. Zhang, *J. Micromech. Microeng.* **2004**, *14*, 1576.
[60] S. Chung, S. Park, *J. Mech. Sci. Technol.* **2013**, *27*, 2701.
[61] R. O. Ritchie, *Nat. Mater.* **2011**, *10*, 817.